mater.scichina.com link.springer.com

Published online 18 November 2020 | https://doi.org/10.1007/s40843-020-1511-7
Sci China Mater 2021, 64(5): 1150–1158

Melamine-assisted synthesis of ultrafine Mo_2C/Mo_2N@N-doped carbon nanofibers for enhanced alkaline hydrogen evolution reaction activity

Jing Chen[1], Anqiang Pan[1*], Wenchao Zhang[2], Xinxin Cao[1], Rou Lu[1], Shuquan Liang[1*] and Guozhong Cao[3*]

ABSTRACT **Noble metal-free electrocatalysts with high activity are highly desirable for the large-scale application of hydrogen evolution reaction (HER). Mo_2C-based nanomaterials have been proved as a promising alternative to noble metal-based electrocatalysts owing to the Pt-resembled d-band density and optimal intermediates-adsorption properties. However, the aggregation and excessive growth of crystals often occur during their high-temperature synthesis procedure, leading to low catalytic utilization. In this study, the ultrafine Mo_2C/Mo_2N heterostructure with large surface and interface confined in the N-doped carbon nanofibers (N-CNFs) was obtained by a melamine-assisted method. The synergistic effect of Mo_2C/Mo_2N heterostructure and plenty active sites exposed on the surface of ultrafine nanocrystals improves the electrocatalytic activity. Meanwhile, the N-CNFs ensure fast charge transfer and high structural stability during reactions. Moreover, the *in-situ* synthesis method strengthens the interfacial coupling interactions between Mo_2C/Mo_2N heterostructure and N-CNFs, further enhancing the electronic conductivity and electrocatalytic activity. Owing to these advantages, Mo_2C/Mo_2N@N-CNFs exhibit excellent HER performance with a low overpotential of 75 mV at a current density of 10 mV cm^{-2} in alkaline solution, superior to the single-phased Mo_2C counterpart and recently reported Mo_2C/Mo_2N-based catalysts. This study highlights a new effective strategy to design efficient electrocatalysts *via* integrating heterostructure, nanostructure and carbon modification.**

Keywords: Mo_2C, hydrogen evolution reaction, heterostructure, ultrafine, nanofibers

INTRODUCTION

Hydrogen (H_2) is a renewable and abundant energy carrier that is regarded as a promising substitute for non-renewable fossil fuels in the future [1–3]. Electrochemical water splitting is considered as one of the most promising hydrogen production techniques, which can be divided into two half-reactions: the oxygen evolution reaction (OER) and hydrogen evolution reaction (HER) [3–7]. However, the practical application of HER is limited by its large overpotential. Interest in searching electrocatalysts has been arising recently. Pt-based electrocatalysts can effectively accelerate the electrochemical process of HER, but it is too scarce and expensive to generalize [8,9]. Therefore, the key challenge to large-scale H_2 production lies in developing low-cost and highly efficient electrocatalysts based on earth-abundant elements.

Transition metal compounds have been widely studied as electrocatalysts for HER in recent years [10,11]. Among these compounds, Mo_2C and Mo_2N are outstanding due to their similar d-band density with Pt, good hydrophilia and chemical stability [12–14], hence, arising concentrated interests. For example, NiO/β-Mo_2C/reduced graphene oxide (RGO) [15], α-MoC [16], and Mo_2C-Mo_3C_2 [17] were synthesized and employed as electrocatalysts to achieve high HER performance. However, most excellent HER catalytic activity was reported in acid media, where HER starts from a favorable process: $2H_3O^+ + 2e^- + M \rightarrow H_{ad} + 2H_2O$ [18,19]. So far, the production of H_2 in the industry conducted under alkaline conditions, in which the HER starts from a more

[1] State Key Laboratory of Powder Metallurgy, School of Materials Science and Engineering, Central South University, Changsha 410083, China
[2] Institute for Superconducting & Electronic Materials, School of Mechanical, Materials, Mechatronics & Biomedical Engineering, Faculty of Engineering and Information Sciences, University of Wollongong, NSW 2500, Australia
[3] Department of Materials Science & Engineering, University of Washington, 98195, WA, USA
* Corresponding authors (emails: pananqiang@csu.edu.cn (Pan A); lsq@csu.edu.cn (Liang S); gzcao@u.washington.edu (Cao G))

thermodynamically difficult process: $2H_2O + 2e^- + M \rightarrow 2M\text{-}H_{ad} + 2OH^-$ [18,19]. Thus, the development of Mo_2C- or Mo_2N-based electrocatalysts with enhanced catalytic activity for HER in alkaline solution is highly imperative. Nevertheless, the traditional synthesis methods of Mo_2C or Mo_2N always suffer from excessive growth and aggregation at high temperatures, which lead to the low utilization of catalysts [13,20–22].

To date, the main effective strategy is compositing nanostructured Mo_2C or Mo_2N with carbon substrate to increase edge-sites and electronic conductivity [23–26]. Song *et al.* [27] prepared N-doped carbon nanotubes (CNTs)-supported Mo_2C nanoparticles, which exhibited outstanding HER performance. The Mo_2C nanoparticles possess high electrocatalytic activity and the N-doped CNTs ensure fast electron transfer. It is generally considered that electrocatalytic reactions always occur at the surface and interface, so the electrocatalytic properties essentially depend on the composition and surface structure, which are always associated with heterostructure, element doping and ultrafine nanosize [28–30]. Therefore, to maximize the utilization of electrocatalysts, ultrafine Mo_2C or Mo_2N crystals are expected to expose more edge sites. Meanwhile, heterostructures with abundant interface or element doping also improve the catalytic activity through the modified electronic state [31–36]. For example, He *et al.* [37] designed Mo_2C-MoO_x on carbon cloth in which the carbon cloth provided high conductivity and Mo_2C-MoO_x heterojunction improved the catalytic activity, resulting in enhanced HER performance compared with the single phase counterparts. However, the crystals that grow on the surface of carbon cloth tend to fall off during long-time reaction, resulting in instability. And the intrinsic electrocatalytic activity of MoO_x in HER is inferior to that of Mo_2C as a candidate component to construct the heterostructure. As same as Mo_2C, Mo_2N possesses Pt-resembled d-band density, which makes the synthesis of Mo_2C/Mo_2N heterostructure attractive [12–14]. However, the construction of ultrafine molybdenum carbide/nitride heterostructure within nitrogen-rich carbon is difficult and has rarely been reported up to now.

In this study, an ultrafine Mo_2C/Mo_2N heterostructure evenly confined with N-doped carbon nanofibers (Mo_2C/Mo_2N@N-CNFs) was fabricated *via* melamine-assisted electrospinning technique and subsequent thermal treatments as illustrated in Fig. 1. Polyacrylonitrile (PAN) was employed as the carbon source to form Mo_2C and carbon nanofibers. As the nitrogen source, small melamine molecules can encircle molybdenum ions in solution by electrostatic interaction, which not only facilitates the *in-situ* introduction of Mo_2N, but also prevents Mo_2C crystals from excessive growth. Ultrafine Mo_2C/Mo_2N heterostructure provides large surface and interface, hence, facilitating the exposure of active sites and ensuring short mass diffusion paths. The nitrogen-rich doped CNF coating benefits fast electron transfer and structure stability. Moreover, the *in-situ* formed $Mo_2C/$

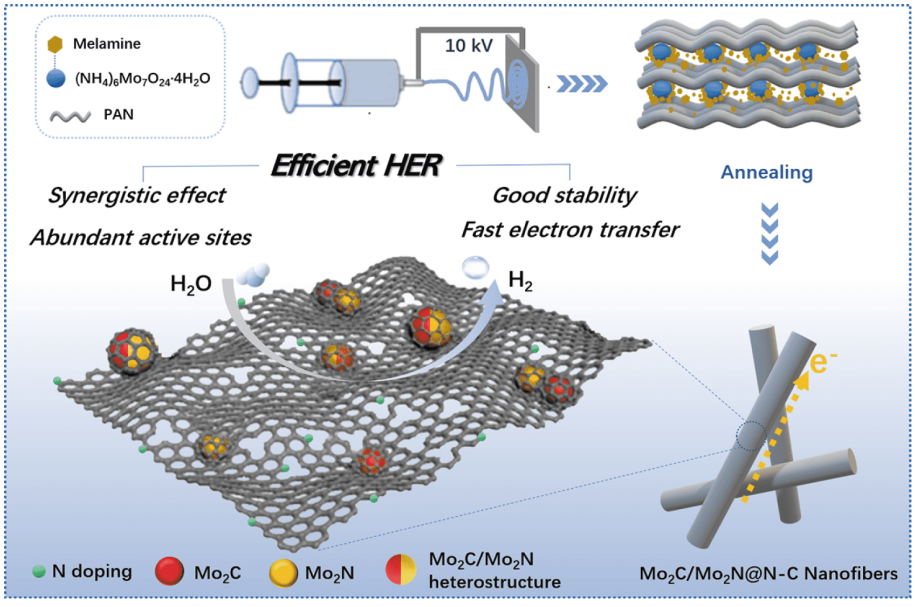

Figure 1 Schematic illustration of the synthesis method and the structure of Mo_2C/Mo_2N@N-CNFs.

Mo_2N from N-C precursor results in the strong contact between the nanocrystals and the N-C substrate, further facilitating the electron transport during the HER process. As expected, the Mo_2C/Mo_2N@N-CNFs display high electrocatalytic activity in alkaline media, such as a low overpotential of 75 mV, which is much superior to that of Mo_2C@N-CNFs. Moreover, it also shows competitive performance among recently reported Mo_2C- or Mo_2N-based electrocatalysts in HER.

EXPERIMENTAL SECTION

Synthesis of Mo_2C@N-CNFs and Mo_2C/Mo_2N@N-CNFs

All chemical reagents and solvents were used as received without further purification. Platinum carbon was purchased from Alfa Aesar. The rest of the chemicals were bought from Aladdin. In an optimized synthesis, 0.20 g of $(NH_4)_6Mo_7O_{24}{\cdot}4H_2O$, 0.15 g melamine and 0.4 g of polyacrylonitrile (PAN, *M*w = 1,500,000) were dissolved in 5 mL of *N*,*N*-dimethylformamide (DMF) with stirring for 12 h to form a homogeneous solution. Then, the solution was inhaled into an injector with a stainless steel needle followed by electrospinning treatment at 10 kV. The flow rate was 5 μL min^{-1} and an aluminum foil 15 cm from the needle was used to collect the sample. Finally, the as-collected sample was directly carbonized under Ar atmosphere at 800°C for 4 h with a heating rate of 5°C min^{-1} to obtain Mo_2C/Mo_2N@N-CNFs. For comparison, the Mo_2C@N-CNFs were synthesized in the same way without adding melamine into the solution.

Materials characterization

The X-ray diffraction (XRD, Rigaku D/max 2500) patterns, Raman spectra (Raman microscope, Horiba Jobin Yvon, Lab Ram Aramis), X-ray photoelectron spectroscopy (XPS, AXIS-ULTRA DLD-600W system), scanning electron microscopy (SEM, Quanta FEG 250), transmission electron microscopy (TEM, JEOL JEM-2100F) images, high-resolution TEM (HRTEM) images, selected area electron diffraction (SAED) image and energy dispersive X-ray (EDX) element mapping data were performed to investigate the crystal structure, chemical composition and morphologies of the as-synthesized samples.

Electrode fabrication and electrochemical measurements

The electrochemical measurements were carried out in a typical three-electrode system attached to a CHI660C workstation at room temperature. Carbon rod and a saturated calomel electrode (Hg/Hg_2Cl_2 in saturated KCl, SCE) were used as counter and reference electrodes, respectively. For working electrodes, first, the as-synthesized catalysts and PVDF powder in a weight ratio of 9:1 in *N*-methyl-2-pyrrolidone (NMP) were mixed to form a homogeneous suspension. Then, the suspension was spread uniformly onto Ni foam and dried at 60°C in vacuum for 6 h. The loading of catalysts for each electrode was about 2 mg cm^{-2}. The electrolyte was 1.0 mol KOH aqueous solution. Linear sweep voltammetry (LSV) was recorded at a scan rate of 5 mV s^{-1} and the initial electric potential was set as −0.1 V *vs.* reversible hydrogen electrode (RHE). The conversion from the measured potential *vs.* $Hg/HgCl_2$ electrode to the potential *vs.* RHE follows Nernst equation: E (*vs.* RHE) = E (*vs.* $Hg/HgCl_2$) + 0.05916pH + 0.244 V. Tafel Plots can be calculated from the corresponding LSV curves. Tafel slopes were fitted to Tafel equation ($\eta = b\log(j) + a$, where η, b and j stand for the overpotential, Tafel slope and current density, respectively).The long-life time test was carried out by *i-t* curve at a constant working potential of −1.30 V for 20 h. Electrochemical impedance spectroscopy (EIS) was tested at the open-circuit voltage with frequency from 0.01 to 1,000,000 Hz and an amplitude of 10 mV. Cycle voltammetry (CV) measurements were conducted in a voltage region from 0.1 to 0.2 V at various scan rates of 10, 20, 40, 60, 80, 100, 120, 140, 160, 180 and 200 mV s^{-1} to obtain the double-layer capacitance (C_{dl}).

RESULTS AND DISCUSSION

Fig. 2a shows the XRD patterns of the as-synthesized samples. For Mo_2C@N-CNFs, diffraction peaks at 34.4°, 37.9°, 39.4°, 52.1°, 61.5°, 69.6°, and 74.6° are ascribed to (100), (002), (101), (102), (110), (103), and (112) planes of Mo_2C (JCPDS No. 35-0787), respectively. The weak broad peak at around 25.0° can be attributed to the carbon in the composite. For Mo_2C/Mo_2N@N-CNFs, except for the peaks of Mo_2C, peaks at 37.7°, 43.2°, 64.1°, and 74.5° are observed, which can be assigned to (112), (200), (204), and (312) planes of Mo_2N (JCPDS No. 25-1368), indicating the formation of Mo_2C/Mo_2N in the composite. In addition, compared with sharp peaks in Mo_2C@N-CNFs, the broaden peaks in Mo_2C/Mo_2N@N-CNFs implying the smaller crystal size. In Raman spectra (Fig. 2b), both samples show the characteristic bands of carbon at 1350 (D-band) and 1580 cm^{-1} (G-band), which arise from the disordered carbon structure and ordered sp^2 carbon structure, respectively [17,34]. The intensity ratio of the D and G bands of Mo_2C/Mo_2N@N-CNFs ($I_D/I_G \approx 1.146$) is higher than that of Mo_2C@N-CNFs ($I_D/I_G \approx 1.064$), demonstrating that the addition of nitrogen successfully increased the defect of carbon in the

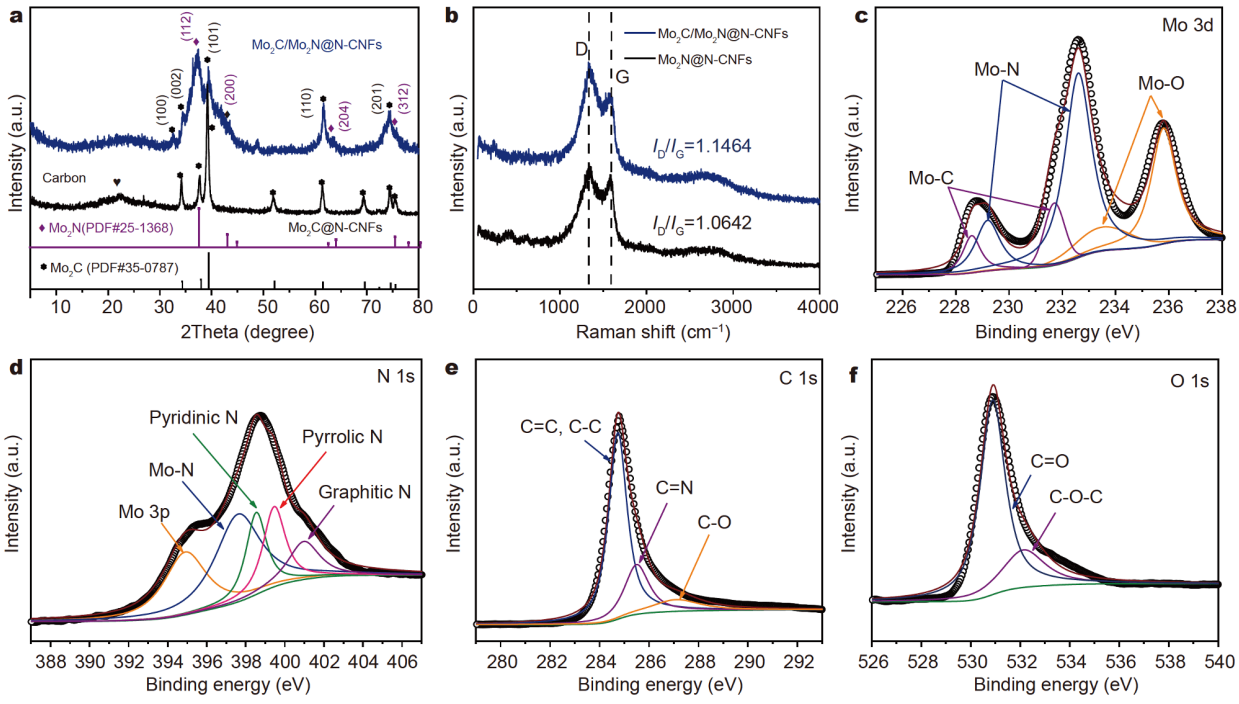

Figure 2 (a) XRD patterns and (b) Raman spectra of Mo_2C@N-CNFs and Mo_2C/Mo_2N@N-CNFs; (c) Mo 3d, (d) N 1s, (e) C 1s, and (f) O 1s XPS spectra of Mo_2C/Mo_2N@N-CNFs.

composite.

To get further insight into the chemical composition of Mo_2C/Mo_2N@N-CNFs and electron effect between Mo_2C, Mo_2N and N-CNFs, XPS was conducted. The XPS survey spectrum shows the presence of Mo, C, N, and O elements in Mo_2C/Mo_2N@N-CNFs (Fig. S1, Supplementary information). As shown in Fig. 2c, the Mo 3d spectrum can be deconvoluted into six doublets, corresponding to Mo–C (228.4/231.5 eV), Mo–N (229.1/232.1 eV), and Mo–O (233.3/235.8 eV) [38–41]. Compared with Mo–C, the Mo atom with Mo–N bond exhibits higher chemical valence states, which may show better catalytic activity, and the Mo–O bond can be ascribed to oxidation of the surface exposed to air. The spectrum of N 1s (Fig. 2d) is resolved to four pairs of peaks. Except for three peaks corresponding to pyridinic N (398.5 eV), pyrrolic N (399.4 eV) and graphitic N (401.4 eV), the peak located at 397.5 eV can also be observed, corresponding to Mo–N species [41,42]. In terms of peak area, pyridinic N and pyrrolic N are the dominating types of doped N, which are beneficial to the electronic conduction and catalysis. By the way, the Mo 3p peak located at 394.9 eV is next to the N 1s spectra. The C 1s spectrum demonstrates the presence of C=C, C–C (284.8 eV), C=N (285.5 eV), and C–O (287.2 eV) bonds in the carbon substrate [34,42], verifying the N-doping in carbon again. And this assignment is also consistent with the spectrum of O 1s in Fig. 2f.

The morphology and structure of the as-synthesized nanofibers were investigated in detail. As depicted in Fig. 3a and Fig. S2, both Mo_2C@N-CNFs and Mo_2C/Mo_2N@N-CNFs possess uniform fibrous morphology with about 100 nm in diameter, inheriting the structure of the precursor after electrospinning (Fig. S3). Fig. 3b shows that Mo_2C@N-CNFs is denser in the center of nanofibers than Mo_2C/Mo_2N@N-CNFs. When we zoom in, the enlarged view (Fig. 3c) clearly shows that dense block of Mo_2C aggregated and was wrapped in the center of carbon nanofibers. The HRTEM of it (Fig. 3d, e) discloses d-spacing of 2.6 Å in the lattice fringes, corresponding to the (100) plane of Mo_2C. And a thick carbon layer uniformly coats around the crystal. The SAED patterns confirm the dense block is Mo_2C multi-crystal again. Interestingly, the internal morphology structure of Mo_2C/Mo_2N@N-CNFs is obviously different from that of Mo_2C@N-CNFs. As shown in Fig. 3f, numerous nanoparticles were uniformly encapsulated in the carbon nanofibers. It can be concluded that introducing melamine preventing Mo_2C from excessive growth into aggregation bulks. HRTEM (Fig. 3g, i) images disclose d-spacing of 2.6 and 2.4 Å in the lattice fringes, which are representative of the (100) and (112) planes of the Mo_2C

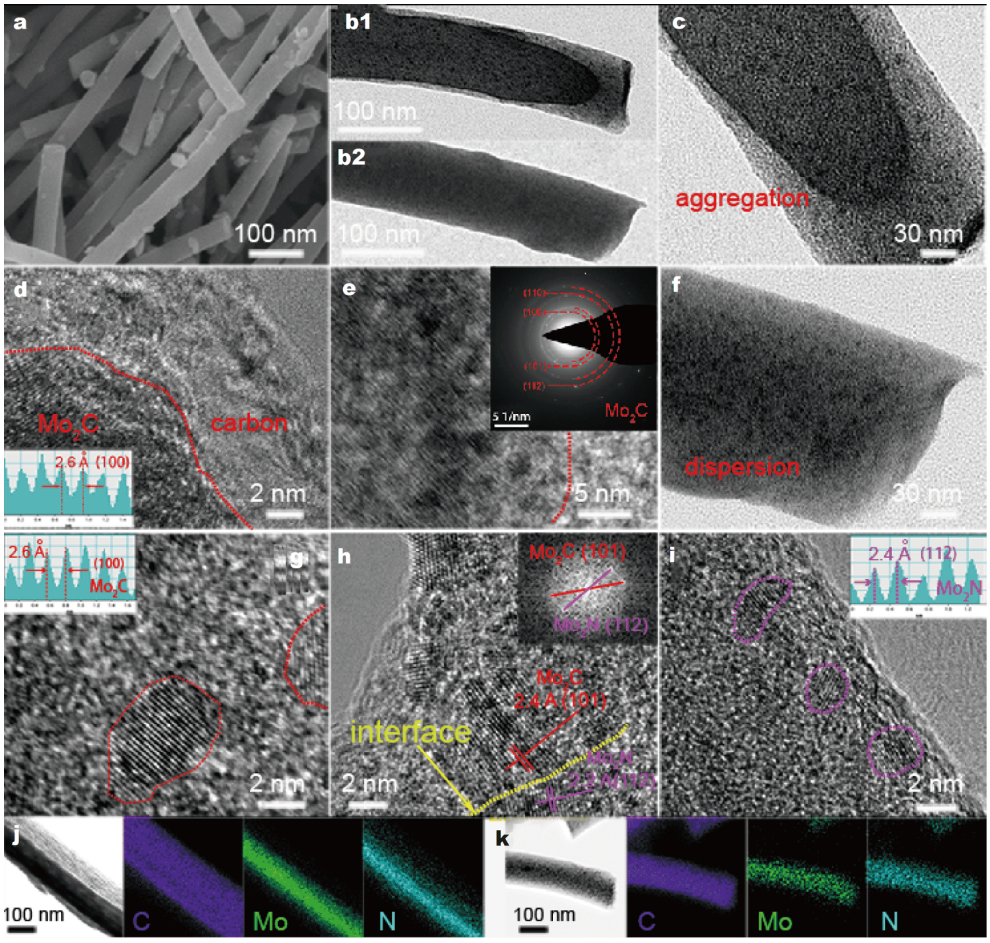

Figure 3 (a) SEM image of Mo_2C/Mo_2N@N-CNFs. TEM images of (b1) Mo_2C@N-CNFs and (b2) Mo_2C/Mo_2N@N-CNFs. TEM image of Mo_2C@N-CNFs: (c) enlarged morphology image, (d, e) HRTEM images. The insets of (d) and (e) show the interplanar spacing of 0.26 nm and SAED pattern of selected regions, respectively. TEM images of Mo_2C/Mo_2N@N-CNFs: (f) morphology image, HRTEM images of (g) Mo_2C crystals, (h) Mo_2C/Mo_2N heterostructure (inset: FFT of the selected area) and (i) Mo_2N crystals in Mo_2C/Mo_2N@N-CNFs sample. Elemental mapping (C, Mo and N) of (j) Mo_2C@N-CNFs and (k) Mo_2C/Mo_2N@N-CNFs sample.

and Mo_2N, respectively, indicating that two phases mixed in the composite. Fig. 3h further illustrates the Mo_2C/Mo_2N heterostructure, where Mo_2C and Mo_2N are intimately connected through the interface (marked by yellow dot line). The corresponding fast Fourier transform (FFT) result (inset in Fig. 3h) confirms that two sides of the interface are the fringes corresponding to the (101) plane of Mo_2C and the (112) plane of Mo_2N, respectively. The interface always induces the optimization of electronic configuration and adsorption free energy through the interfacial electron transfer through heterointerfaces, achieving synergistic effect to improve electrocatalytic activity [13,37]. Fig. 3j confirms again that Mo_2C crystals in Mo_2C@N-CNFs gathered in the center of N-CNFs, while the elemental mapping of Mo_2C/Mo_2N @N-CNFs shows the uniform distribution of elements. The ultrasmall sizes of nanocrystals (mixed Mo_2C and Mo_2N, Mo_2C/Mo_2N heterostructure) in Mo_2C/Mo_2N@N-CNFs, correspond to the result of broad peaks in XRD, which is beneficial for the exposure of active sites on surface, improving the utilization of the catalyst. Meanwhile, the N-doped carbon coating guarantees fast electron transfer and structural stability during long-time reaction [16,42,43].

The HER activity of the obtained catalysts was investigated in 1 mol L^{-1} KOH aqueous solution. Fig. 4a shows the LSVs of Mo_2C@N-CNFs and Mo_2C/Mo_2N@N-CNFs together with the commercial Pt/C as reference. The overpotential (η_{10}, determined by the potential at a current density of 10 mA cm^{-2}) of Mo_2C/Mo_2N@N-CNFs is 75 mV, much smaller than 123 mV of Mo_2C@N-CNFs, indicating a higher electrocatalytic activity. And the

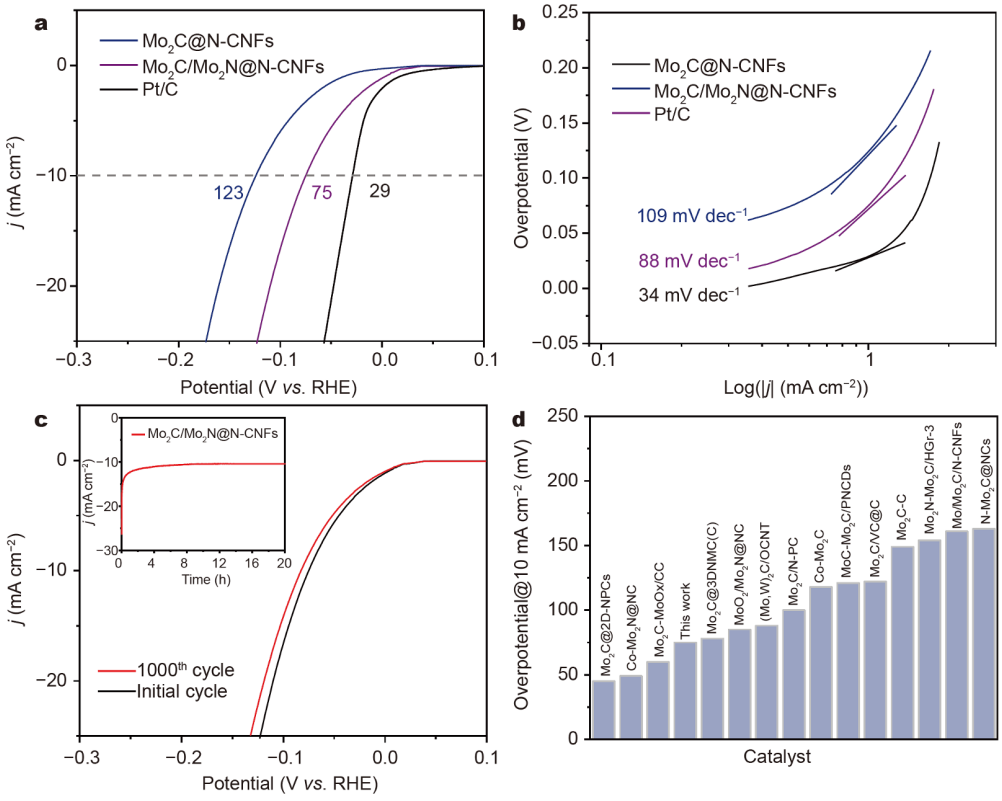

Figure 4 (a) Polarization curves and (b) Tafel slopes of Mo_2C@N-CNFs, Mo_2C/Mo_2N@N-CNFs and the commercial Pt/C. (c) The first and 1000th cycles polarization curves of Mo_2C/Mo_2N@N-CNFs; inset: long term stability at 1.13 V. (d) Comparison of η_{10} of Mo_2C/Mo_2N@N-CNFs with recently reported Mo_xC or Mo_xN based electrocatalysts.

commercial Pt/C shows an overpotential of 29 mV, consistent with the previously reported literature [44,45]. Tafel slope is a crucial parameter to assess the rate-limiting step and kinetics in HER. Volmer, Heyrovsky, and Tafel reactions are three types of rate-limiting steps of HER, where the theoretical values of Tafel slopes are 120, 40 and 30 mV dec^{-1}, respectively [44,45]. As shown in Fig. 4b, the fitting linear portion of Tafel plots was determined to be 10 mA cm^{-2}. Both Mo_2C@N-CNFs and Mo_2C/Mo_2N@N-CNFs possess Tafel slopes less than 120 mV dec^{-1}, but more than 40 mV dec^{-1} (109 and 88 mV dec^{-1}, respectively), indicating the reaction is Volmer-Heyrovsky mechanism. The smaller Tafel slope of Mo_2C/Mo_2N@N-CNFs implies a favorable HER kinetics, representing the faster mass/charge transportation during catalytic reaction [45].

As presented in Fig. 4c, the polarization curves after 1000 cycles and the first cycle are nearly overlapped, and almost no current fluctuation could be observed in 20 h, suggesting the high stability of Mo_2C/Mo_2N@N-CNFs catalyst. It can be proposed that the N-CNFs coating guarantees the high structural stability during long-time HER. Moreover, the η_{10} of Mo_2C/Mo_2N@N-CNFs is comparable to those of other molybdenum carbide/nitride-based materials in alkaline solution recently reported in Fig. 4d and Table S1 [35–44,46–50]. As a result, the ultrafine Mo_2C/Mo_2N heterostructure shows quite superior performance among them, which demonstrates its advantages in electrocatalytic activity of HER.

To further understand the mechanism of the enhanced HER activity of Mo_2C/Mo_2N@N-CNFs electrocatalysts, the electrochemical surface area (ECSA) and charge transfer resistance (R_{ct}) were investigated as displayed in Fig. 5. To evaluate the ECSA of electrocatalysts, we calculated the electrochemical double layer capacitance (C_{dl}) of the electrocatalysts determined from the CV curves tested at different scanning rates from 100–200 mV (Fig. 5a, b). As can be seen in Fig. 5c, the C_{dl} of 30.01 mF cm^{-2} on Mo_2C/Mo_2N@N-CNFs is much higher than that of Mo_2C@N-CNFs (15.25 mF cm^{-2}), which implies a larger density of active sites for HER of the former [17]. The major enriched active sites stem from the interface in heterostructure and edge-sites on the surface of ultrafine Mo_2C/Mo_2N. Meanwhile, their EIS

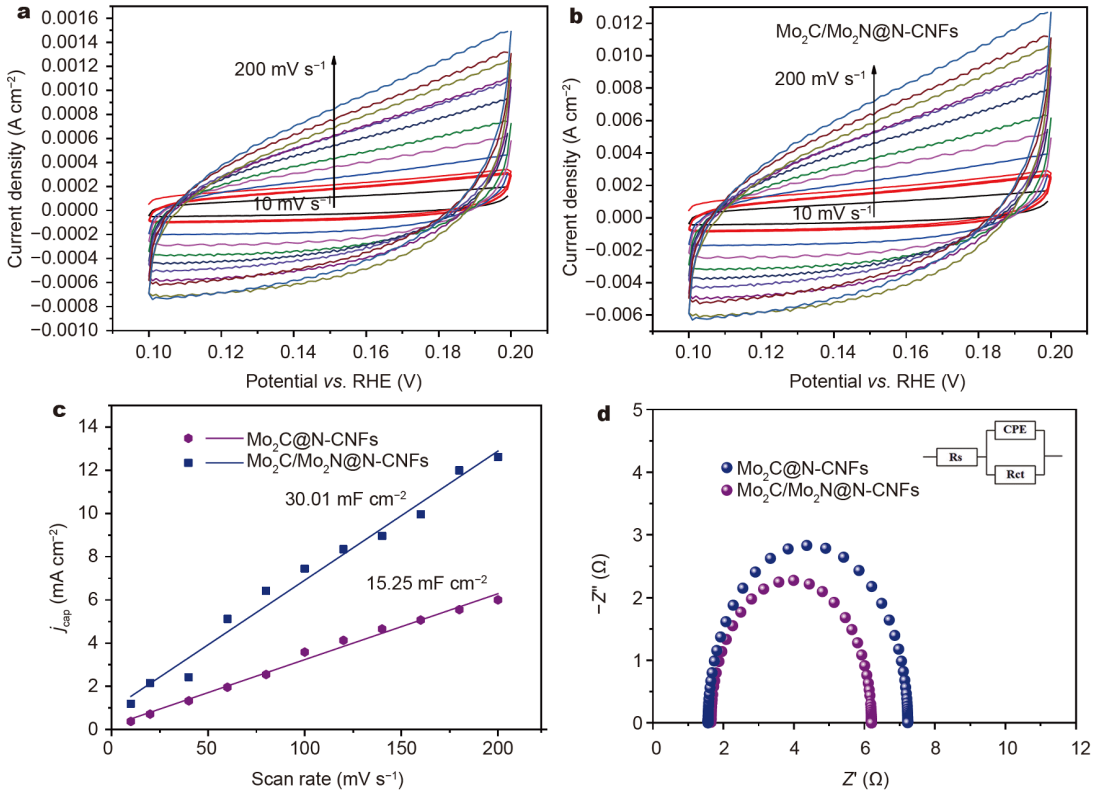

Figure 5 CV curves of (a) Mo_2C@N-CNFs and (b) Mo_2C/Mo_2N@N-CNFs electrodes in the voltage range over 0.1–0.2 V *vs.* SCE at various scan rates. (c) Estimation of C_{dl} of Mo_2C@N-CNFs and Mo_2C/Mo_2N@N-CNFs by plotting the current density variation at 150 mV *vs.* RHE. (d) Nyquist plots of Mo_2C@N-CNFs and Mo_2C/Mo_2N@N-CNFs.

and the corresponding equivalent circuits are shown in Fig. 5d, in which the equivalent resistance of Mo_2C/Mo_2N@N-CNFs is smaller than that of Mo_2C@N-CNFs, demonstrating the Mo_2C/Mo_2N@N-CNFs possess fast charge transfer rate [5]. The improved electronic conductivity of Mo_2C/Mo_2N@N-CNFs can be ascribed to the conductive N-CNFs coating and the strong interaction between Mo_2C/Mo_2N and N-CNFs, which further boosts the HER kinetics.

CONCLUSIONS

In summary, we reported a melamine-assisted facile method to synthesize ultrafine molybdenum carbide/nitride heterostructure encapsulated in N-CNFs for highly efficient HER. By introducing melamine, single-phased Mo_2C or dual-phased Mo_2C/Mo_2N heterostructure can be regulated as well as the ultrafine nanosize. Owing to the synergistic effect of Mo_2C/Mo_2N heterostructure and the abundant active sites from the interface or surface exposed in ultrafine nanocrystals, the as-prepared Mo_2C/Mo_2N@N-CNFs possess excellent HER activity. Moreover, the N-CNFs coating and the intimate contact of Mo_2C/Mo_2N and N-C guarantee fast electron transfer and structure stability, boosting the reaction kinetics. Hence, Mo_2C/Mo_2N@N-CNFs deliver superior HER performance as exemplified by a small overpotential of 75 mV at η_{10}, much better than those of Mo_2C@N-CNFs and other Mo_2C/Mo_2N-based catalysts recently reported.

Received 26 June 2020; accepted 4 September 2020; published online 18 November 2020

1 Zhu C, Fu S, Shi Q, *et al.* Single-atom electrocatalysts. Angew Chem Int Ed, 2017, 56: 13944–13960
2 Zhang X, Shao J, Huang W, *et al.* Three dimensional carbon substrate materials for electrolysis of water. Sci China Mater, 2018, 61: 1143–1153
3 Pan Y, Zhang C, Lin Y, *et al.* Electrocatalyst engineering and structure-activity relationship in hydrogen evolution reaction: From nanostructures to single atoms. Sci China Mater, 2020, 63: 921–948
4 Yang G, Jiao Y, Yan H, *et al.* Interfacial engineering of MoO_2-FeP heterojunction for highly efficient hydrogen evolution coupled with biomass electrooxidation. Adv Mater, 2020, 32: 2000455
5 Qiao C, Rafai S, Cao T, *et al.* Tuning surface electronic structure of two-dimensional cobalt-based hydroxide nanosheets for highly

efficient water oxidation. ChemCatChem, 2020, 12: 2823–2832
6 Qiao C, Zhang Y, Zhu Y, *et al.* One-step synthesis of zinc–cobalt layered double hydroxide (Zn–Co-LDH) nanosheets for high-efficiency oxygen evolution reaction. J Mater Chem A, 2015, 3: 6878–6883
7 Souleymen R, Wang Z, Qiao C, *et al.* Microwave-assisted synthesis of graphene-like cobalt sulfide freestanding sheets as an efficient bifunctional electrocatalyst for overall water splitting. J Mater Chem A, 2018, 6: 7592–7607
8 Liu ZL, Lei B, Zhu ZL, *et al.* Spontaneous formation of 1D pattern in monolayer VSe_2 with dispersive adsorption of Pt Atoms for HER catalysis. Nano Lett, 2019, 19: 4897–4903
9 Bai J, Jia N, Jin P, *et al.* Metal-organic interface engineering for boosting the electroactivity of Pt nanodendrites for hydrogen production. J Energy Chem, 2020, 51: 105–112
10 Meng T, Cao M. Transition metal carbide complex architectures for energy-related applications. Chem Eur J, 2018, 24: 16716–16736
11 Yang Y, Xu X, Wang X. Synthesis of Mo-based nanostructures from organic-inorganic hybrid with enhanced electrochemical for water splitting. Sci China Mater, 2015, 58: 775–784
12 Miao M, Pan J, He T, *et al.* Molybdenum carbide-based electrocatalysts for hydrogen evolution reaction. Chem Eur J, 2017, 23: 10947–10961
13 Ge R, Huo J, Sun M, *et al.* Surface and interface engineering: molybdenum carbide–based nanomaterials for electrochemical energy conversion. Small, 2019, 15: 1903380
14 Huo L, Liu B, Gao Z, *et al.* 0D/2D heterojunctions of molybdenum carbide-tungsten carbide quantum dots/n-doped graphene nanosheets as superior and durable electrocatalysts for hydrogen evolution reaction. J Mater Chem A, 2017, 5: 18494–18501
15 Ni J, Ruan Z, Zhu S, *et al.* Sandwiched NiO/β-Mo_2C/RGO as improved electrocatalyst for hydrogen evolution reaction: solvothermal-assisted self-assembly and catalytic mechanism. ChemElectroChem, 2019, 6: 5958–5966
16 Deng Y, Gao R, Lin L, *et al.* Solvent tunes the selectivity of hydrogenation reaction over α-MoC catalyst. J Am Chem Soc, 2018, 140: 14481–14489
17 Jia L, Li C, Zhao Y, *et al.* Interfacial engineering of Mo_2 C–Mo_3C_2 heteronanowires for high performance hydrogen evolution reactions. Nanoscale, 2019, 11: 23318–23329
18 Subbaraman R, Tripkovic D, Strmcnik D, *et al.* Enhancing hydrogen evolution activity in water splitting by tailoring Li^+-$Ni(OH)_2$-Pt interfaces. Science, 2011, 334: 1256–1260
19 Xiao P, Sk MA, Thia L, *et al.* Molybdenum phosphide as an efficient electrocatalyst for the hydrogen evolution reaction. Energy Environ Sci, 2014, 7: 2624–2629
20 Kang Q, Qin Y. Lu Q, *et al.* Waste leather-derived (Cr, N)-co-doped carbon cloth coupling with Mo_2C nanoparticles as a self-supported electrode for highly active hydrogen evolution reaction performances. J Power Sources, 2020, 476: 228706
21 Patel M, Subrahmanyam J. Synthesis of nanocrystalline molybdenum carbide (Mo_2C) by solution route. Mater Res Bull, 2008, 43: 2036–2041
22 Halim J, Kota S, Lukatskaya MR, *et al.* Synthesis and characterization of 2D molybdenum carbide (MXene). Adv Funct Mater, 2016, 26: 3118–3127
23 Xiong T, Jia J, Wei Z, *et al.* N-doped carbon-wrapped Mo_2C heterophase sheets for high-efficiency electrochemical hydrogen production. Chem Eng J, 2019, 358: 362–368
24 Zou Y, Ma D, Sun D, *et al.* Carbon nanosheet facilitated charge separation and transfer between molybdenum carbide and graphitic carbon nitride toward efficient photocatalytic H_2 production. Appl Surf Sci, 2019, 473: 91–101
25 Zhou Z, Yuan Z, Li S, *et al.* Big to small: ultrafine Mo_2C particles derived from giant polyoxomolybdate clusters for hydrogen evolution reaction. Small, 2019, 15: 1900358
26 Cheng R, He H, Pu Z, *et al.* Shrunken hollow Mo-N/Mo-C nanosphere structure for efficient hydrogen evolution in a broad pH range. Electrochim Acta, 2019, 298: 799–805
27 Song YJ, Ren JT, Yuan G, *et al.* Facile synthesis of Mo_2C nanoparticles on N-doped carbon nanotubes with enhanced electrocatalytic activity for hydrogen evolution and oxygen reduction reactions. J Energy Chem, 2019, 38: 68–77
28 Hu X, Zhang W, Liu X, *et al.* Nanostructured Mo-based electrode materials for electrochemical energy storage. Chem Soc Rev, 2015, 44: 2376–2404
29 Yang S, Wang Y, Zhang H, *et al.* Unique three-dimensional Mo_2C@MoS_2 heterojunction nanostructure with S vacancies as outstanding all-pH range electrocatalyst for hydrogen evolution. J Catal, 2019, 371: 20–26
30 Yang Y, Luo M, Xing Y, *et al.* A universal strategy for intimately coupled carbon nanosheets/mom nanocrystals (M = P, S, C, and O) hierarchical hollow nanospheres for hydrogen evolution catalysis and sodium-ion storage. Adv Mater, 2018, 30: 1706085
31 Zhang W, Hu C, Guo Z, *et al.* High-performance K-CO_2 batteries based on metal-free carbon electrocatalysts. Angew Chem Int Ed, 2020, 59: 3470–3474
32 Jian C, Cai Q, Hong W, *et al.* Edge-riched $MoSe_2$/MoO_2 hybrid electrocatalyst for efficient hydrogen evolution reaction. Small, 2018, 14: 1703798
33 Zhang W, Liu Y, Guo Z. Approaching high-performance potassium-ion batteries *via* advanced design strategies and engineering. Sci Adv, 2019, 5: eaav7412
34 Chen J, Pan A, Wang Y, *et al.* Hierarchical mesoporous $MoSe_2$@CoSe/N-doped carbon nanocomposite for sodium ion batteries and hydrogen evolution reaction applications. Energy Storage Mater, 2019, 21: 97–106
35 Fu Q, Peng B, Masa J, *et al.* Synergistic effect of molybdenum and tungsten in highly mixed carbide nanoparticles as effective catalysts in the hydrogen evolution reaction under alkaline and acidic conditions. ChemElectroChem, 2020, 7: 983–988
36 Kumar R, Rai R, Gautam S, *et al.* Nano-structured hybrid molybdenum carbides/nitrides generated *in situ* for her applications. J Mater Chem A, 2017, 5: 7764–7768
37 He L, Zhang W, Mo Q, *et al.* Molybdenum carbide-oxide heterostructures: *in situ* surface reconfiguration toward efficient electrocatalytic hydrogen evolution. Angew Chem Int Ed, 2020, 59: 3544–3548
38 Lu C, Tranca D, Zhang J, *et al.* Molybdenum carbide-embedded nitrogen-doped porous carbon nanosheets as electrocatalysts for water splitting in alkaline media. ACS Nano, 2017, 11: 3933–3942
39 Lu XF, Yu L, Zhang J, *et al.* Ultrafine dual-phased carbide nanocrystals confined in porous nitrogen-doped carbon dodecahedrons for efficient hydrogen evolution reaction. Adv Mater, 2019, 1900699
40 Lv Z, Tahir M, Lang X, *et al.* Well-dispersed molybdenum nitrides on a nitrogen-doped carbon matrix for highly efficient hydrogen evolution in alkaline media. J Mater Chem A, 2017, 5: 20932–20937

41 Lang X, Qadeer MA, Shen G, *et al.* A Co–Mo_2N composite on a nitrogen-doped carbon matrix with hydrogen evolution activity comparable to that of Pt/C in alkaline media. J Mater Chem A, 2019, 7: 20579–20583
42 Han W, Chen L, Ma B, *et al.* Ultra-small Mo_2C nanodots encapsulated in nitrogen-doped porous carbon for pH-universal hydrogen evolution: insights into the synergistic enhancement of HER activity by nitrogen doping and structural defects. J Mater Chem A, 2019, 7: 4734–4743
43 An K, Xu X. Mo_2C based electrocatalyst with nitrogen doped three-dimensional mesoporous carbon as matrix, synthesis and her activity study. Electrochim Acta, 2019, 293: 348–355
44 Huang C, Miao X, Pi C, *et al.* Mo_2C/VC heterojunction embedded in graphitic carbon network: An advanced electrocatalyst for hydrogen evolution. Nano Energy, 2019, 60: 520–526
45 Lee J, Kim C, Choi KS, *et al. In-situ* coalesced vacancies on $MoSe_2$ mimicking noble metal: Unprecedented Tafel reaction in hydrogen evolution. Nano Energy, 2019, 63: 103846
46 Lin H, Liu N, Shi Z, *et al.* Cobalt-doping in molybdenum-carbide nanowires toward efficient electrocatalytic hydrogen evolution. Adv Funct Mater, 2016, 26: 5590–5598
47 Li G, Yu J, Zhou Z, *et al.* N-doped Mo_2C nanobelts/graphene nanosheets bonded with hydroxy nanocellulose as flexible and editable electrode for hydrogen evolution reaction. iScience, 2019, 19: 1090–1100
48 Yan H, Xie Y, Jiao Y, *et al.* Holey reduced graphene oxide coupled with an Mo_2N-Mo_2C heterojunction for efficient hydrogen evolution. Adv Mater, 2018, 30: 1704156
49 Wu Z, Wang J, Liu R, *et al.* Facile preparation of carbon sphere supported molybdenum compounds (P, C and S) as hydrogen evolution electrocatalysts in acid and alkaline electrolytes. Nano Energy, 2017, 32: 511–519
50 Li M, Wang H, Zhu Y, *et al.* Mo/Mo_2C encapsulated in nitrogen-doped carbon nanofibers as efficiently integrated heterojunction electrocatalysts for hydrogen evolution reaction in wide pH range. Appl Surf Sci, 2019, 496: 143672

Acknowledgements This work was supported by the National Natural Science Foundation of China (51932011, 51872334, 51874326 and 51572299), the Natural Science Foundation of Hunan Province for Distinguished Young Scholars (2018JJ1036), and the Independent Exploration and Innovation Project for graduate students of the Central South University (2019zzts049).

Author contributions Chen J performed the experiments and wrote the article; Cao X and Lu R participated in the experiments; Zhang W performed the data analysis; Pan A, Liang S and Cao G proposed the experimental design. All authors contributed to the general discussion.

Conflict of interest The authors declare no conflict of interest.

Supplementary information Experimental details and supporting data are available in the online version of the paper.

Jing Chen received her MSc degree from the School of Materials Science and Engineering, Central South University in 2017. Currently, she is a PhD candidate at the Central South University. Her current research focuses on Mo-based materials for energy storage and conversion.

Anqiang Pan received his BE (2005) and PhD (2011) degrees in materials physics and chemistry from the Central South University. In 2008, he worked in Prof. Guozhong Cao's group at the University of Washington as an exchange student (2008–2009). Then, he got the chance to work in PNNL as a visiting scholar in Dr. Ji-Guang Zhang and Dr. Jun Liu's group (2009–2011). After getting his PhD degree, he joined Prof. Xiongwen (David) Lou's group at Nanyang Technological University as a research fellow (2011–2012). He joined the faculty at the Central South University in 2012 and was promoted to a Sheng-Hua Professor in 2013. His current interests are controllable synthesis of nanostructured materials and their applications in energy storage and conversion devices, such as LIBs, and supercapacitors.

Shuquan Liang received his PhD degree from the Central South University in 2000. He has been the Dean of the School of Materials Science and Engineering, Central South University since 2010. He is the winner of Monash University Engineering Sir John Medal. He has published more than 100 peer-reviewed papers. Currently, his main research interests include micro/nano-structured functional materials, nanocomposites and their energy storage and conversion devices.

氮掺杂碳纳米纤维包覆超细碳化钼/氮化钼异质结构用于碱性条件下电催化析氢

陈婧[1], 潘安强[1*], 张文超[2], 曹鑫鑫[1], 卢柔[1], 梁叔全[1*], 曹国忠[3*]

摘要 高效非贵金属催化剂对于推进析氢反应(HER)的大规模工业化至关重要. 碳化钼(Mo_2C)因其类似铂的能带密度和优良的中间产物吸附特性, 有望替代贵金属基材料成为具有前景的催化剂. 然而, 它在常规制备过程中存在严重的晶体过度生长和团聚问题, 导致催化效率低. 本研究利用三聚氰胺辅助法制备了含有丰富表面和界面的超细碳化钼/氮化钼(Mo_2C/Mo_2N)异质结构, 并同时将其嵌入到氮掺杂碳纳米纤维(CNFs)中. Mo_2C/Mo_2N异质结构的协同作用与超细纳米晶表面暴露的丰富活性位点共同提高了电催化活性, 而氮掺杂碳纳米纤维框架保证了快速的电荷转移和良好的结构稳定性. 此外, 原位形成的Mo_2C/Mo_2N晶体与碳基质之间存在较强的界面耦合作用, 进一步提高了电子电导率和电催化活性. 得益于这些优势, Mo_2C/Mo_2N@N-CNFs在碱性溶液中表现出优异的电催化析氢性能, 在电流密度10 mV cm^{-2}时具有75 mV的低过电势, 优于单相Mo_2C@N-CNFs对比样以及近期报道的Mo_2C/Mo_2N基催化剂. 这个合成方法集成了异质结构、纳米化和碳修饰策略, 为设计高效率电催化材料提供了新的参考.

